Early Transition Metals Strengthen the B_2 Bond in MB_2 Complexes

Journal:	*Journal of the American Chemical Society*
Manuscript ID	ja-2021-13709a.R3
Manuscript Type:	Communication
Date Submitted by the Author:	n/a
Complete List of Authors:	Merriles, Dakota; University of Utah, Department of Chemistry Tomchak, Kimberly; University of Utah, Department of Chemistry Nielson, Christopher; University of Utah, Department of Chemistry Morse, Michael; University of Utah, Department of Chemistry

Early Transition Metals Strengthen the B_2 Bond in MB_2 Complexes

Dakota M. Merriles, Kimberly H. Tomchak, Christopher Nielson, and Michael D. Morse*

Department of Chemistry, University of Utah, Salt Lake City, Utah 84112, United States

KEYWORDS: Metals, Ligands, Chemical Structure, Metal Clusters, Quantum Mechanics

ABSTRACT: The bond dissociation energies of early transition metal diborides (M-B_2, M = Sc, Ti, V, Y, Mo) have been measured by observation of the sharp onset of predissociation in a highly congested spectrum. Density functional and CCSD(T) *ab initio* calculations, extrapolated to the complete basis set limit, have been used to examine the electronic structure of these species. The computations demonstrate the formation of bonding orbitals between the metal *d* orbitals and the $1\pi_u$ bonding orbitals of B_2, leading to the transfer of metallic electron density into the bonding $1\pi_u$ orbitals, strengthening both the M-B and B-B bonds in the molecule. This runs counter to most metal-ligand π interactions, where electron density is generally transferred into π antibonding orbitals of the ligand.

The Dewar-Chatt-Duncanson (DCD) bonding model is a key concept explaining the bonding between transition metals and ligands having π-bonds. Briefly, the LUMO of the transition metal accepts a σ-type donation of electron density from the HOMO of the π-bonded ligand, while concurrently, the electron density in the HOMO of the transition metal is donated into the vacant LUMO (π-antibonding symmetry) of the ligand.[1] This synergistic bonding mechanism activates the ligand by weakening its bond, as found in transition metal carbonyls, olefins, and alkynes.[2] In these compounds, the hallmark of π-backbonding is a universal increase in bond length and decrease in fundamental stretching frequency of the ligand when it is metal-bound *versus* when its isolated.[3-5] Additionally, the π orbitals of the ligand that engage in π-backbonding can be either oriented perpendicular to the metal-ligand axis or parallel to it, although the former is more common.[2, 6] The DCD bonding model has been widely accepted as the most useful concept for understanding the bonding between the transition metal and ligands with π-bonds.[7-8]

The first report of an apparent violation of the DCD bonding model was realized by Braunschweig *et al* during the computational study and ensuing synthesis of the platinum-centered diborene complex, $(Et_3P)_2Pt(B_2Duryl_2)$ in 2013.[9] This apparent violation occurs because in forming the complex, two π bonding SOMOs on the diborene are combined with two singly occupied *d* orbitals on the Pt atom to form two doubly-occupied bonding orbitals in a closed shell singlet state. In the process electron density is transferred from Pt to the π bonding orbitals of the diborene, strengthening both the M-B and B-B bonds. The measured B-B bond length in the $(Et_3P)_2Pt(B_2Duryl_2)$ complex is exceptionally short, 1.510(14) Å. This is the opposite of what is regularly observed in the DCD model, illustrating that a different bonding scheme is obtained when the interaction with the π-bonded ligand occurs via a bonding orbital, rather than an antibonding orbital . Since this discovery, there has been interest in augmenting and replicating this bonding mechanism with theoretical calculations on various other metallaboron complexes.[10-11] However, the platinum-centered diborene complex $(Et_3P)_2Pt(B_2Duryl_2)$ remains the sole experimental demonstration of the strengthening of the boron-boron bond via M → B_2 π-bonding interaction. Because this has only been experimentally achieved using the electron-rich late transition metal Pt, it is unknown if the electron deficient early transition metals may also be able to strengthen a π-bonded diboron ligand via a similar mechanism.

Here, we report that the electron deficient early transition metals (M= Sc, Ti, V, Y, Zr Nb, Mo, Hf, Ta, W) mediate an increase in the bond strength of a diboron ligand in the context of the early transition metal diboride complexes, MB_2. Owing to advancements in experimental techniques and the development of accurate computational methods, size-selected transition metal doped boron clusters have been shown to engage in a wide array of bonding schemes, motifs, and geometries.[12-15] However, noticeably absent from the literature are experimental studies on the family of neutral transition metal diboride (MB_2) species. In the present work, we systematically study a series of MB_2 species to examine whether the early transition metals can bond with B_2 by interaction with the B_2 $1\pi_u$ bonding orbitals and to build a bridge between the recently acquired knowledge of MB and MB_3 species.[15-22] Through accurate spectroscopic measurements of their predissociation thresholds and quantum chemical computations, we have confirmed that the bonding scheme proposed by Braunschweig for the Pt-diborene complexes remains valid for the early transition metal MB_2 molecules.

In previous work,[21-38] we have demonstrated that for small *d*- and *f*-block molecules, the high density of electronic states in the vicinity of the ground separated fragment limit allows the molecule to dissociate via spin-orbit and nonadiabatic couplings[39] as soon as this limit is exceeded in energy, leading to a sharp drop in the ion

signal obtained in a resonant two-photon ionization (R2PI) spectroscopy experiment. As illustrated in Figures 1 and S1-S5, this method has allowed us to measure the predissociation thresholds of ScB_2, TiB_2, VB_2, YB_2, and MoB_2. A thermochemical cycle described in the SI demonstrates that the measured bond dissociation energies correspond to breaking the M-B_2 bond, leaving the B_2 fragment intact. On this basis we assign BDEs of the MB_2 species as: D_0(Sc-B_2) = 4.17(3) eV, D_0(Ti-B_2) = 4.623(5) eV, D_0(V-B_2) = 4.590(5) eV, D_0(Y-B_2) = 4.663(5) eV, and D_0(Mo-B_2) = 4.917(20) eV, where the assigned error limit is given in parentheses. Details are provided in the SI. Attempts were made to measure the BDEs of ZrB_2, NbB_2, HfB_2, TaB_2, and WB_2, but the expected sharp drops in ion signal were not observed at energies below 5.30 eV, the practical upper limit of our laser system at the time. From this, we conclude that the BDEs of these latter molecules are greater than 5.30 eV.

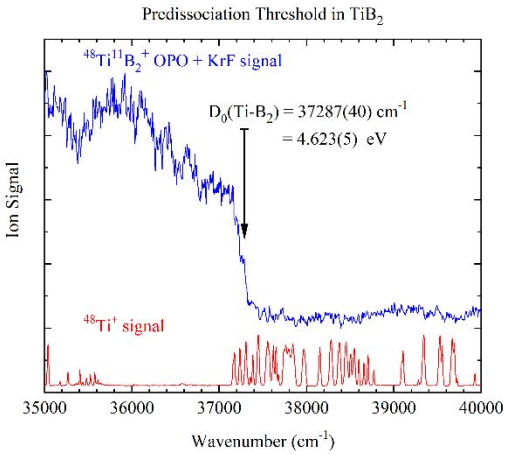

Figure 1. R2PI spectrum of TiB_2 (top trace) with its predissociation threshold at 37287(40) cm^{-1}. The atomic spectrum of Ti (lower trace) was used for calibration. The horizontal bar atop the arrow displays the ±40 cm^{-1} assigned error limit.

To examine the bonding in these molecules and investigate whether the bonding in the B_2 subunit is strengthened, we performed UB3LYP/aug-cc-pVQZ(-PP) calculations to elucidate the ground state electronic structures and global minima of the early MB_2 species studied here (details in the SI).[40-43] First, the electronic energies of various structural isomers were probed to determine the global minimum of each MB_2 molecule. Two linear geometries were calculated: one in which the transition metal is between the boron atoms (B-M-B) and one in which the B_2 entity remained intact and bonded end-on (M-B-B). A cyclic C_{2v} geometry was also calculated. For all of the MB_2 species, the cyclic C_{2v} geometry was confirmed as the global minimum. Figure S6 illustrates each geometry that was calculated for the MB_2 species using ScB_2 as the example. Table S1 displays the measured and calculated BDEs (obtained by CCSD(T) methods extrapolated to the complete basis set limit), calculated ionization energies (CCSD(T)/aug-cc-pVQZ(-PP)), ground terms, and ground electronic configurations for all of the early transition metal MB_2 molecules. The energetic differences between the calculated structural isomers and the global minimum structure at the UB3LYP/aug-cc-pVQZ(-PP) level are tabulated in Table S2.

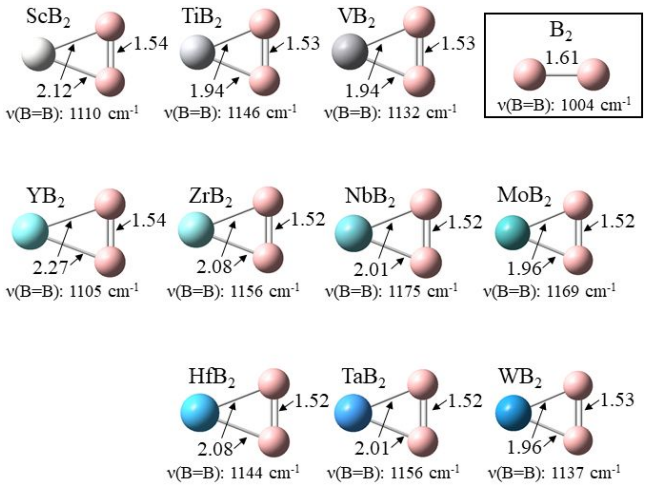

Figure 2. Calculated global minima geometries of the MB_2 and B_2 species calculated at the UB3LYP/B, Sc, Ti, V (aug-cc-pVQZ)/Y, Zr, Nb, Mo, Hf, Ta, W (aug-cc-pVQZ-PP) level of theory. The respective bond lengths of each molecule are given in Å units and the frequency of the symmetric stretch of the two boron atoms is given underneath each structure. Experimental measurements on the B_2 ground state give a bond length and harmonic frequency of 1.587 Å and 1053 cm^{-1}, respectively.[44]

Figure 2 shows the global minimum geometries of each MB_2 species as well as that of the bare diboron ligand (also see Table S3). The cyclic C_{2v} geometry of these molecules is identical to the structural disposition of the platinum atom and diborene ligand in the $(Et_3P)_2Pt(B_2Duryl_2)$ complex. Therefore, a similar bonding mechanism may be occurring in these early transition metal diborides.

Images of each MO for TiB_2 in its calculated $^1A_1$ electronic ground state (Figure S7) also describe the generated MOs for all of the early MB_2 molecules, although electronic occupancies of the higher-energy MOs of course vary. The $1b_1$ and $2a_1$ MOs (see Figure 3) are the relevant MOs for possible bonding between a *d* orbital on the transition metal and the $1\pi_u$ bonding orbitals on diboron. These are bonding orbitals between the metal and the diboron, and within the B_2 unit as well. From the calculated ground electronic configurations (Table S1), it may be noted that the $1b_1$ and $2a_1$ MOs are doubly occupied in each molecule, giving a strong bonding interaction between the transition metal and the diboron ligand. As the $1\pi_u$ orbitals of B_2 are doubly occupied, two of the electrons occupying these orbitals come from B_2, two from the metal; thus, electron donation from both centers occurs. For a more quantitative analysis of the chemical bonding in each MB_2, specifically for the $1b_1$ and $2a_1$ MOs, an orbital composition analysis for each MO was performed using a full natural bond orbital analysis.[45-46] The results are listed in Table 1. These show that there is interaction between the relevant transition metal orbitals and the bonding $1\pi_u$ orbitals of the diboron molecule confirming the existence of both coplanar and orthogonal bonding in these complexes.

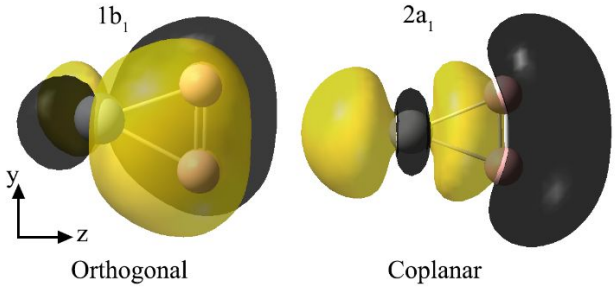

Figure 3. TiB_2's $1b_1$ and $2a_1$ molecular orbitals, which demonstrate strongly bonding interactions between the Ti πd_{xz} orbital and the $1\pi_u$ bonding orbital of diboron in the $1b_1$ MO, and the Ti dz^2/s orbitals and the remaining $1\pi_u$ bonding orbital of diboron in the $2a_1$ MO.

Table 1. Orbital composition analysis of the $1b_1$ and $2a_1$ MO in the early transition metal diborides

	$1b_1$ Molecular Orbital		$2a_1$ Molecular Orbital	
	% M πd_{xz}	% B_2 $1\pi_u$	% M $\sigma d_z^2, s$	% B_2 $1\pi_u$
ScB_2	26	73	10, 13	69
TiB_2	48	50	34, 15	34
VB_2	86	12	5, 14	80
YB_2	23	56	12, 6	77
ZrB_2	40	29	34, 20	43
NbB_2	72	22	12, 12	74
MoB_2	83	17	10, 14	70
HfB_2	34	65	35, 11	53
TaB_2	56	44	19, 12	48
WB_2	74	25	8, 19	70

The $1b_2$ orbital of the MB_2 complexes also contributes to the bonding in these molecules. It combines the filled $1\sigma_u$ antibonding orbital of B_2 (mainly $2s$) with the d_{yz} of the metal, leading to partial electron donation from B_2 to the metal. The transfer of electron density out of the $1\sigma_u$ antibonding orbital strengthens the B-B bond. Similarly, the $3a_1$ orbital is a bonding combination of the metal d_{z2} orbital with the empty $2\sigma_g$ (mainly $2p_z$) orbital of B_2, leading to metal to B_2 electron donation. The increase in occupation of $3a_1$ from one electron (ScB_2 and YB_2) to two electrons in the later members of their periods causes a corresponding increase in M-B_2 BDE. These orbitals are displayed in Figure 4; compositions are given in Table S5.

Further evidence that the B-B bond is strengthened in these species may be found in Figure 2, where all ten early transition metal diborides exhibit a calculated B=B vibrational frequency that is 10-17% greater than isolated B_2, as well as a calculated B-B bond length that is shortened by 0.07 to 0.09 Å. Similarly, the bond energy of the B_2 unit within the MB_2 molecules may be judged by the energy required to break the cyclic molecules into linear BMB species. These are all calculated (Table S2) to be greater than the BDE of B_2 (2.75 eV)[47] by 0.25 to 2.46 eV. All of these measures demonstrate enhanced B-B bonding in the early transition metal MB_2 complexes, consistent with the donation of metallic electron density into the B_2 $1\pi_u$ bonding orbitals and donation of B_2 antibonding electron density from the $1\sigma_u$ orbital into empty metal d orbitals. In contrast, other early transition metal- and lanthanide-X_2 (X= C, N, O, P) molecules show a universal weakening of the X_2 bond, consistent with the DCD model of electron donation into the π^* antibonding orbital.[48-54]

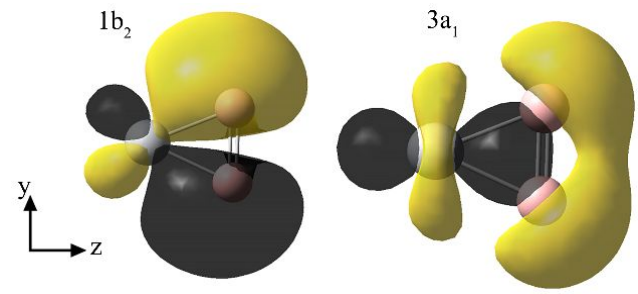

Figure 4. TiB_2's $1b_2$ and $3a_1$ orbitals, like the $1b_1$ and $2a_1$ orbitals, contribute to strengthening the M-B_2 bond.

It is noteworthy that after the exclusion of NbB_2, for reasons described in the SI, the M-B_2 BDEs follow a trend line where on average there is a 133±3% increase in BDE compared to the corresponding metal monoboride BDEs (Table S4 and Figure S8). The fact that the BDEs of the MB_2 molecules are more than double the BDEs of the monoborides is at least partially due to the occupancy of the $2a_1$ and $1b_1$ MOs, which provide both M-B and B-B bonding interactions.

To conclude, spectroscopic results show an impressive increase in strength of the transition-metal boron bond in the MB_2 molecules as compared to the MB species. Likewise, computational results show significant strengthening of the B-B bond when an early transition metal is bonded to diboron. Chemical bonding analysis shows bonding interaction between the metal d orbitals and the diboron $1\pi_u$-bonding orbitals in the $1b_1$ and $2a_1$ MOs, as well as significant donation of B_2 $1\sigma_u$ antibonding density into the empty metallic d_{yz} orbital in the $1b_2$ orbital. We hope that these results help to inspire further research and new insights in metalloboron chemistry.

ASSOCIATED CONTENT

The supporting information material is available free of charge at http://pubs.acs.org/doi/xxx: In-depth descriptions of the experimental and computational methods employed in this study; the R2PI spectra of ScB_2, TiB_2, VB_2, YB_2, and MoB_2; molecular orbital diagram of TiB_2; calculated isomers of the MB_2 species; comparisons of the BDEs of MB *vs.* MB_2; calculated BDEs, ionization energies, and ground electronic states of the MB_2 molecules; and calculated structural information of the MB_2 molecules.

AUTHOR INFORMATION

Corresponding Author

* **Michael D. Morse** – Department of Chemistry, University of

Utah, Salt Lake City, Utah 84112, United States;
https://orcid.org/0000-0002-2386-7315;
Email: morse@chem.utah.edu; Fax: (801)-581-8433

Authors

Dakota M. Merriles – Department of Chemistry, University of Utah, Salt Lake City, Utah 84112, United States;
https://orcid.org/0000-0003-1363-1306
Kimberly H. Tomchak – Department of Chemistry, University of Utah, Salt Lake City, Utah 84112, United States;
https://orcid.org/0000-0001-5403-0086
Christopher Nielson – Department of Chemistry, University of Utah, Salt Lake City, Utah 84112, United States;
https://orcid.org/0000-0001-7260-3423

Notes

The authors declare no competing financial interest.

ACKNOWLEDGMENT

The authors thank the National Science Foundation for support of this research under Grant No. CHE-1952924. The authors would also like to express gratitude to Brandon C. Stevenson for his assistance with the calculations performed in this work. The authors also thank the Center for High Performance Computing at the University of Utah for their technical resources and support.

REFERENCES

1. Dewar–Chatt–Duncanson Bonding Model. In *Encyclopedia of Inorganic and Bioinorganic Chemistry*, Scott, R. A., Ed. 2011.
2. Cotton, F. A.; Wilkinson, G., *Advanced Inorganic Chemistry*. 3rd ed.; Wiley: New York, 1972; p 1145.
3. Goodman, H.; Mei, L.; Gianetti, T. L., Molecular Orbital Insights of Transition Metal-Stabilized Carbocations. *Frontiers in Chemistry* **2019,** *7* (365), 1-19.
4. Bistoni, G.; Rampino, S.; Scafuri, N.; Ciancaleoni, G.; Zuccaccia, D.; Belpassi, L.; Tarantelli, F., How π back-donation quantitatively controls the CO stretching response in classical and non-classical metal carbonyl complexes. *Chem. Sci.* **2016,** *7* (2), 1174-1184.
5. Frenking, G.; Fernández, I.; Holzmann, N.; Pan, S.; Krossing, I.; Zhou, M., Metal–CO Bonding in Mononuclear Transition Metal Carbonyl Complexes. *JACS Au* **2021,** *1* (5), 623-645.
6. Rakowsky, M. H.; Woolcock, J. C.; Wright, L. L.; Green, D. B.; Rettig, M. F.; Wing, R. M., In-plane coordinated double bonds. Molecular structures, spectroscopy, and stability of 5-methylenecyclooctene and 5-methylenecycloheptene complexes of platinum(II). *Organometallics* **1987,** *6* (6), 1211-1218.
7. Mingos, D. M. P., A historical perspective on Dewar's landmark contribution to organometallic chemistry. *Journal of Organometallic Chemistry* **2001,** *635* (1), 1-8.
8. Frenking, G., The Dewar–Chatt–Duncanson bonding model of transition metal-olefin complexes examined by modern quantum chemical methods. In *Modern coordination chemistry: the legacy of Joseph Chatt*, Leigh, G. J.; Winterton, N., Eds. Royal Society of Chemistry: London, 2002; pp 111-122.
9. Braunschweig, H.; Damme, A.; Dewhurst, R. D.; Vargas, A., Bond-strengthening π backdonation in a transition-metal π-diborene complex. *Nature Chemistry* **2013,** *5* (2), 115-121.
10. Ghorai, S.; Jemmis, E. D., A DFT Study on the Stabilization of the B≡B Triple Bond in a Metallaborocycle: Contrasting Electronic Structures of Boron and Carbon Analogues. *Chemistry – A European Journal* **2017,** *23* (41), 9746-9751.
11. Hari Krishna Reddy, K.; Jemmis, E. D., Stabilization of diborane(4) by transition metal fragments and a novel metal to π Dewar–Chatt–Duncanson model of back donation. *Dalton Transactions* **2013,** *42* (29), 10633-10639.
12. Li, W.-L.; Chen, X.; Jian, T.; Chen, T.-T.; Li, J.; Wang, L.-S., From planar boron clusters to borophenes and metalloborophenes. *Nature Reviews Chemistry* **2017,** *1* (10), 0071.
13. Sergeeva, A. P.; Popov, I. A.; Piazza, Z. A.; Li, W.-L.; Romanescu, C.; Wang, L.-S.; Boldyrev, A. I., Understanding Boron through Size-Selected Clusters: Structure, Chemical Bonding, and Fluxionality. *Acc. Chem. Res.* **2014,** *47* (4), 1349-1358.
14. Jian, T.; Chen, X.; Li, S.-D.; Boldyrev, A. I.; Li, J.; Wang, L.-S., Probing the structures and bonding of size-selected boron and doped-boron clusters. *Chemical Society Reviews* **2019,** *48* (13), 3550-3591.
15. Cheung, L. F.; Kocheril, G. S.; Czekner, J.; Wang, L.-S., Observation of Mobius Aromatic Planar Metallaborocycles. *J. Am. Chem. Soc.* **2020,** *142* (7), 3356-3360.
16. Cheung, L. F.; Czekner, J.; Kocheril, G. S.; Wang, L.-S., High-resolution photoelectron imaging of MnB_3^-: Probing the bonding between the aromatic B_3 cluster and 3d transition metals. *J. Chem. Phys.* **2020,** *152* (24), 244306.
17. Czekner, J.; Cheung, L. F.; Kocheril, G. S.; Kulichenko, M.; Boldyrev, A. I.; Wang, L.-S., High-Resolution Photoelectron Imaging of IrB_3^-: Observation of a π-Aromatic B_3^+ Ring Coordinated to a Transition Metal. *Angew. Chem., Int. Ed.* **2019,** *58* (26), 8877-8881.
18. Cheng, S.-B.; Berkdemir, C.; Castleman, A. W., Observation of d–p hybridized aromaticity in lanthanum-doped boron clusters. *Phys. Chem. Chem. Phys.* **2014,** *16* (2), 533-539.
19. Li, W.-L.; Ivanov, A. S.; Federic, J.; Romanescu, C.; Cernusak, I.; Boldyrev, A. I.; Wang, L.-S., On the way to the highest coordination number in the planar metal-centred aromatic $Ta©B_{10}^-$ cluster: Evolution of the structures of TaB_n^- (n = 3-8). *J. Chem. Phys.* **2013,** *139* (10), 104312.
20. Chen, Q.; Bai, H.; Zhai, H.-J.; Li, S.-D.; Wang, L.-S., Photoelectron spectroscopy of boron-gold alloy clusters and boron boronyl clusters: $B_3Au_n^-$ and $B_3(BO)_n^-$ (n = 1, 2). *J. Chem. Phys.* **2013,** *139* (4), 044308.
21. Merriles, D. M.; Nielson, C.; Tieu, E.; Morse, M. D., Chemical Bonding and Electronic Structure of the Early Transition Metal Borides: ScB, TiB, VB, YB, ZrB, NbB, LaB, HfB, TaB, and WB. *J. Phys. Chem. A* **2021,** *125* (20), 4420-4434.
22. Merriles, D. M.; Tieu, E.; Morse, M. D., Bond Dissociation Energies of FeB, CoB, NiB, RuB, RhB, OsB, IrB, and PtB. *J. Chem. Phys.* **2019,** *151*, 044302.
23. Merriles, D. M.; Tomchak, K. H.; Ewigleben, J. C.; Morse, M. D., Predissociation measurements of the bond dissociation energies of EuO, TmO, and YbO. *J. Chem. Phys.* **2021,** *155* (14), 144303.
24. Sorensen, J. J.; Tieu, E.; Morse, M. D., Bond dissociation energies of lanthanide sulfides and selenides. *J. Chem. Phys.* **2021,** *154*, 124307.
25. Sorensen, J. J.; Tieu, E.; Sevy, A.; Merriles, D. M.; Nielson, C.; Ewigleben, J. C.; Morse, M. D., Bond dissociation energies of transition metal oxides: CrO, MoO, RuO, and RhO. *J. Chem. Phys.* **2020,** *153*, 074303.
26. Merriles, D. M.; Sevy, A.; Nielson, C.; Morse, M. D., The bond dissociation energy of VO measured by resonant three-photon ionization spectroscopy. *J. Chem. Phys.* **2020,** *153*, 024303.
27. Sorensen, J. J.; Tieu, E.; Morse, M. D., Bond dissociation energies of the diatomic late transition metal sulfides: RuS, OsS, CoS, RhS, IrS, and PtS. *J. Chem. Phys.* **2020,** *152*, 244305.
28. Sorensen, J. J.; Tieu, E.; Morse, M. D., Bond dissociation energies of diatomic transition metal selenides: ScSe, YSe, RuSe, OsSe, CoSe, RhSe, IrSe, and PtSe. *J. Chem. Phys.* **2020,** *152*, 124305.
29. Sorensen, J. J.; Tieu, E.; Nielson, C.; Sevy, A.; Tomchak, K. H.; Morse, M. D., Bond dissociation energies of diatomic transition metal sulfides: ScS, YS, TiS, ZrS, HfS, NbS, and TaS. *J. Chem. Phys.* **2020,** *152*, 194307.
30. Sevy, A.; Merriles, D. M.; Wentz, R. S.; Morse, M. D., Bond Dissociation Energies of ScSi, YSi, LaSi, ScC, YC, LaC, CoC, and YCH. *J. Chem. Phys.* **2019,** *151*, 024302.

31. Morse, M. D., Predissociation Measurements of Bond Dissociation Energies. *Acc. Chem. Res.* **2019,** *52*, 119-126.
32. Sevy, A.; Tieu, E.; Morse, M. D., Bond Dissociation Energies of FeSi, RuSi, OsSi, CoSi, RhSi, IrSi, NiSi, and PtSi. *J. Chem. Phys.* **2018,** *149*, 174307.
33. Sevy, A.; Huffaker, R. F.; Morse, M. D., Bond Dissociation Energies of Tungsten Molecules: WC, WSi, WS, WSe, and WCl. *J. Phys. Chem. A* **2017,** *121* (49), 9446-9457.
34. Sevy, A.; Matthew, D. J.; Morse, M. D., Bond dissociation energies of TiC, ZrC, HfC, ThC, NbC, and TaC. *J. Chem. Phys.* **2018,** *149* (4), 044306.
35. Matthew, D. J.; Tieu, E.; Morse, M. D., Determination of the bond dissociation energies of FeX and NiX (X = C, S, Se). *J. Chem. Phys.* **2017,** *146*, 144310.
36. Sorensen, J. J.; Persinger, T. D.; Sevy, A.; Franchina, J. A.; Johnson, E. L.; Morse, M. D., Bond dissociation energies of diatomic transition metal selenides: TiSe, ZrSe, HfSe, VSe, NbSe, and TaSe. *J. Chem. Phys.* **2016,** *145* (21), 214308.
37. Sevy, A.; Sorensen, J. J.; Persinger, T. D.; Franchina, J. A.; Johnson, E. L.; Morse, M. D., Bond dissociation energies of diatomic transition metal silicides: TiSi, ZrSi, HfSi, VSi, NbSi, and TaSi. *J. Chem. Phys.* **2017,** *147* (8), 084301.
38. Johnson, E. L.; Davis, Q. C.; Morse, M. D., Predissociation measurements of bond dissociation energies: VC, VN, and VS. *J. Chem. Phys.* **2016,** *144* (23), 234306.
39. Lefebvre-Brion, H.; Field, R. W., Chapter 6 - Predissociation. In *Perturbations in the Spectra of Diatomic Molecules*, Lefebvre-Brion, H.; Field, R. W., Eds. Academic Press: 1986; pp 331-382.
40. Becke, A. D., Density-functional thermochemistry. III. The role of exact exchange. *J. Chem. Phys.* **1993,** *98* (7), 5648-52.
41. Raghavachari, K.; Trucks, G. W.; Pople, J. A.; Head-Gordon, M., A fifth-order perturbation comparison of electron correlation theories. *Chem. Phys. Lett.* **1989,** *157* (6), 479-483.
42. Peterson, K. A.; Woon, D. E.; Dunning, T. H., Benchmark calculations with correlated molecular wave functions. IV. The classical barrier height of the $H+H_2 \rightarrow H_2+H$ reaction. *J. Chem. Phys.* **1994,** *100* (10), 7410-7415.
43. Feller, D.; Peterson, K. A.; Grant Hill, J., On the effectiveness of CCSD(T) complete basis set extrapolations for atomization energies. *J. Chem. Phys.* **2011,** *135* (4), 044102.
44. Bredohl, H.; Dubois, I.; Nzohabonayo, P., The emission spectrum of B_2. *J. Mol. Spectrosc.* **1982,** *93* (2), 281-5.
45. Reed, A. E.; Curtiss, L. A.; Weinhold, F., Intermolecular interactions from a natural bond orbital, donor-acceptor viewpoint. *Chem. Rev.* **1988,** *88* (6), 899-926.
46. Lu, T.; Chen, F., Multiwfn: A multifunctional wavefunction analyzer. *J. Comput. Chem.* **2012,** *33* (5), 580-592.
47. Miliordos, E.; Mavridis, A., An accurate first principles study of the geometric and electronic structure of B_2, B_2^-, B_3, B_3^-, and B_3H: Ground and excited states. *J. Chem. Phys.* **2010,** *132* (16), 164307.
48. Halfen, D. T.; Min, J.; Ziurys, L. M., The Fourier transform microwave spectrum of YC_2 (X^2A_1) and its ^{13}C isotopologues: Chemical insight into metal dicarbides. *Chem. Phys. Lett.* **2013,** *555*, 31-37.
49. Redondo, P.; Barrientos, C.; Largo, A., Small Carbon Clusters Doped with Vanadium Metal: A Density Functional Study of VC_n (n = 1-8). *J. Chem. Theory Comput.* **2006,** *2* (3), 885-893.
50. Burton, M. A.; Cheng, Q.; Halfen, D. T.; Lane, J. H.; DeYonker, N. J.; Ziurys, L. M., The structure of ScC2 (X̃2A1): A combined Fourier transform microwave/millimeter-wave spectroscopic and computational study. *The Journal of Chemical Physics* **2020,** *153* (3), 034304.
51. Dai, D.; Roszak, S.; Balasubramanian, K., Electronic States and Potential Energy Surfaces of NbC_2. *J. Phys. Chem. A* **2000,** *104* (24), 5861-5866.
52. Pyykkö, P.; Tamm, T., Calculated Structures of MO_2^{2+}, MN_2, and MP_2 (M = Mo, W). *J. Phys. Chem. A* **1997,** *101* (43), 8107-8114.
53. Brunken, S.; Mueller, H. S. P.; Menten, K. M.; McCarthy, M. C.; Thaddeus, P., The rotational spectrum of TiO_2. *Astrophysical Journal* **2008,** *676* (2, Pt. 1), 1367-1371.
54. Demireva, M.; Armentrout, P. B., Gadolinium cation (Gd^+) reaction with O_2: Potential energy surface mapped experimentally and with theory. *J. Chem. Phys.* **2017,** *146* (17), 174302.

TOC Graphic

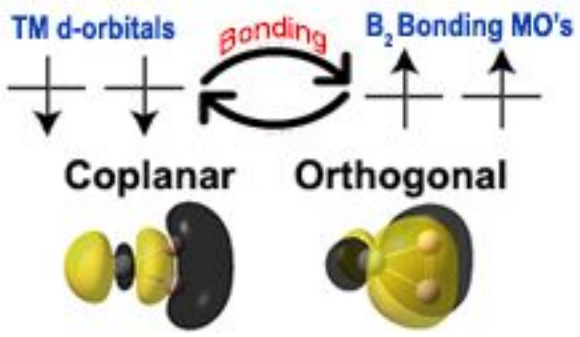

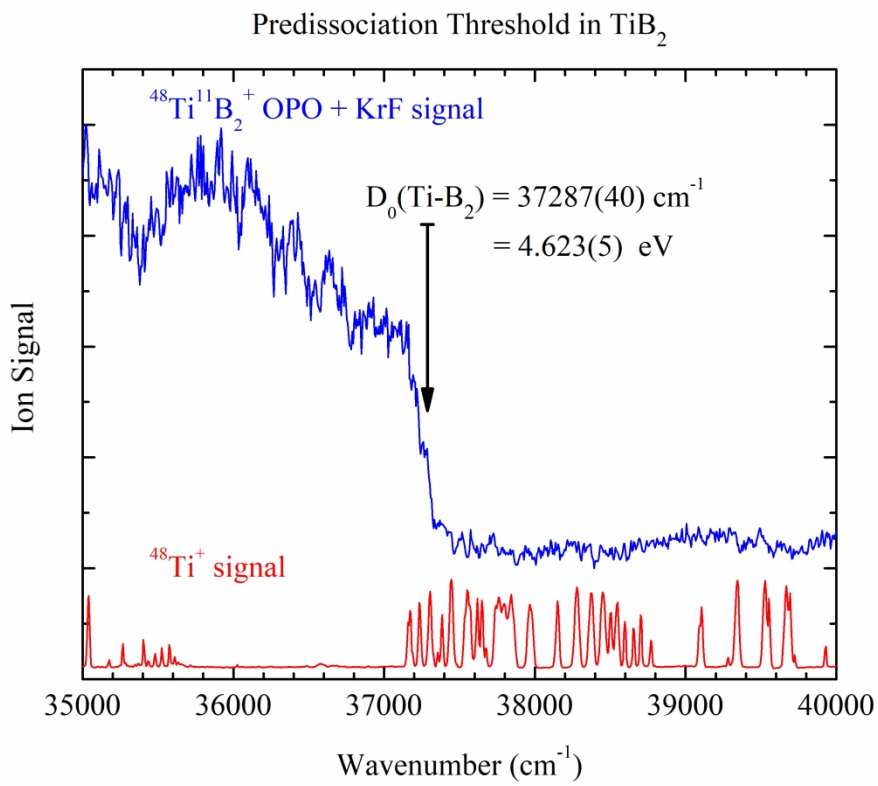

Figure 1. R2PI spectrum of TiB_2 (top trace) with its predissociation threshold at 37287(40) cm^{-1}. The atomic spectrum of Ti (lower trace) was used for calibration.

247x220mm (300 x 300 DPI)

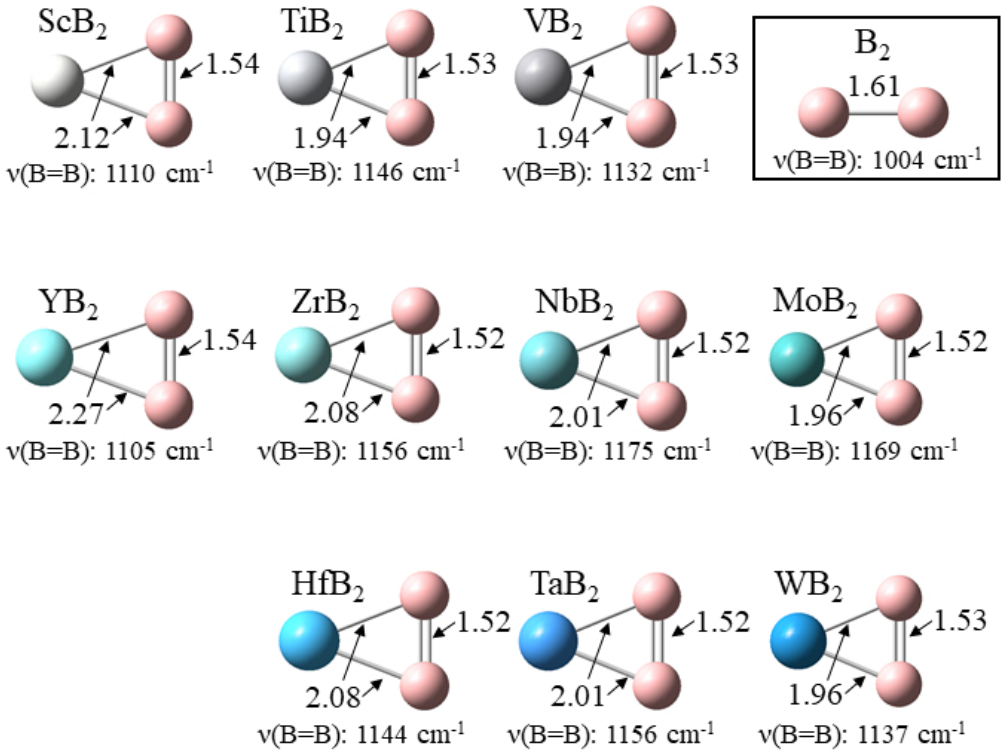

Figure 2. Ground state geometries of the MB_2 and B_2 species calculated at the UB3LYP/B, Sc, Ti, V (aug-cc-pVQZ)/Y, Zr, Nb, Mo, Hf, Ta, W (aug-cc-pVQZ-PP) level of theory. The respective bond lengths of each molecule are given in Å units and the frequency of the symmetrical stretch of the two boron atoms is given underneath each structure. Experimental measurements on the B_2 ground state give a bond length and harmonic frequency of 1.587 Å and 1053 cm^{-1}, respectively.[44]

178x133mm (96 x 96 DPI)

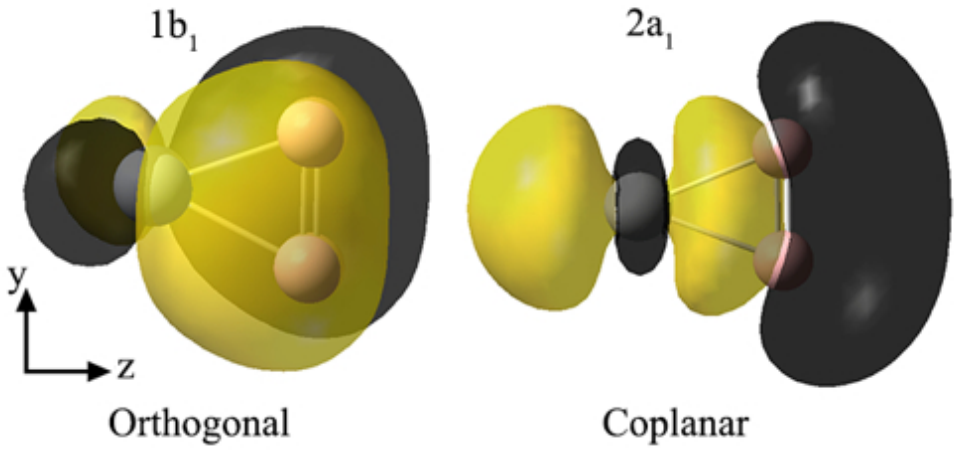

Figure 3. TiB_2's $1b_1$ and $2a_1$ molecular orbitals, which demonstrate strongly bonding interactions between the Ti πd_{xz} orbital and the $1\pi_u$ bonding orbital of diboron in the $1b_1$ MO, and the Ti d_{z2}/s orbitals and the remaining $1\pi_u$ bonding orbital of diboron in the $2a_1$ MO.

177x86mm (72 x 72 DPI)

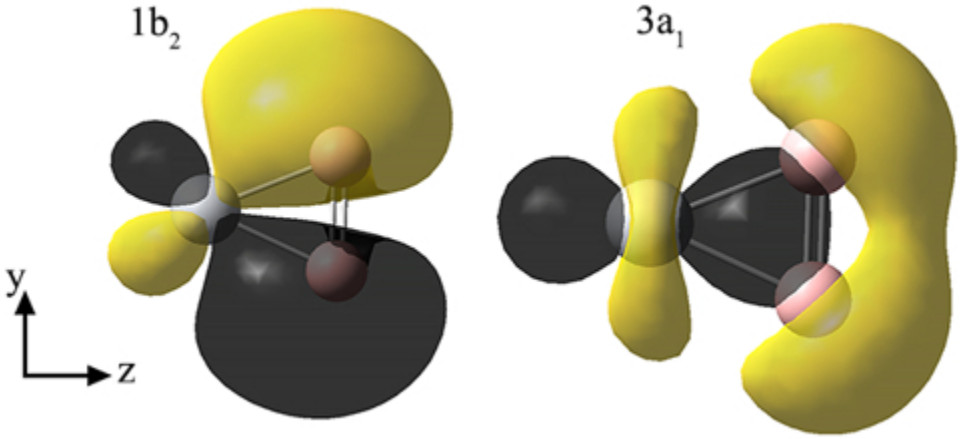

Figure 4. TiB_2's $1b_2$ and $3a_1$ orbitals, like the $1b_1$ and $2a_1$ orbitals, contribute to strengthening the M-B_2 bond.

174x80mm (72 x 72 DPI)

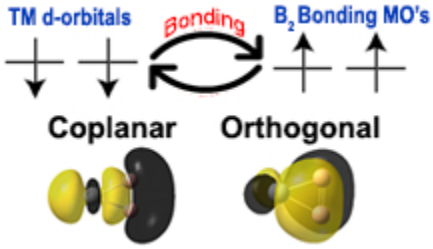

Table of Contents Graphic

82x44mm (72 x 72 DPI)